Approximate Analytical Equations for the Stirrer Angular Correlation in a Reverberation Chamber

Qian Xu, *Member*, *IEEE*, Lei Xing, *Member, IEEE*, Yongjiu Zhao, Tian-Hong Loh, *Senior Member, IEEE,* Min Wang and Yi Huang, *Senior Member, IEEE*

***Abstract*—In a reverberation chamber, the angular correlation coefficient of a stirrer is an important parameter. It has been used to evaluate the performance of a stirrer or to estimate the number of independent samples in a measurement. In the previous work, the angular correlation coefficient was evaluated numerically and no analytical equation has been proposed. In this study we propose an approximate analytical equation to fit the measured angular correlation which shows good agreements with measurement results. General properties of angular correlation coefficient are explored with physical insights, the equivalency of the mean value of the angular correlation and the *K*-factor is revealed. This study provides further understandings on the control of the stirrer angular correlation and the *K*-factor in a reverberation chamber.**

***Index Terms*—Reverberation chamber, *K*-factor, independent positions, stirrer angular correlation.**

I. Introduction

A reverberation chamber (RC) is a highly resonant electrically large cavity with mechanical stirrers used to stir the electromagnetic field inside it [1]. Recently, it has been used for emulating the multipath channel experienced by communication systems, especially for the next generation mobile communication systems (5G) [2-6].

One of the challenging problems in RC measurements is to control the statistical environment in an expected way. Over the years, typical parameters such as Q factor [7-12], power delay profile (PDP) [13, 14], Rician K-factor [15-21] and absorption cross section (ACS) [22-25] have been investigated and analytical expressions have been explored to provide understandings and guidelines to control these variables. The Q factor and the PDP can be tuned by loading the RC using radio absorbing materials (RAMs), while the K-factor can be tuned by using both antennas and the RAMs. The relationships between the Q factor and the ACS of the RAM [1], the K-factor and the radiation pattern of the antenna (including Q factor) [1] have already been obtained.

Although not all parameters in an RC have analytical forms, analytical expressions provide physical insights and help to understand and control the parameters in an RC. The angular correlation coefficient (ACC) is an important parameter to characterize the correlation between different channel realizations in an RC, it can also be used to calculate the number of independent samples of a mechanical stirrer [26-32]. Correlation matrix method has been used to evaluate the number of independent stirrer positions [30-32]. In this study, we propose an approximate analytical expression for the ACC measurement which was often characterized numerically. Some general properties for the ACC are also derived, especially the relationship between the ACC and the K-factor.

This study is organized as follows: Section II gives the definition of the ACC; measurement results and the proposed analytical expression are detailed in Section III. Section IV discusses the general properties of the ACC and links it to the average K-factor in an RC; discussion and conclusions are summarized in Section V.

II. Definition of the Angular Correlation Coefficient

A schematic plot of an RC is illustrated in Fig. 1. Ant 1 and Ant 2 are antennas connected to port 1 and port 2 of a vector network analyzer (VNA) respectively; two stirrers are driven by stepper motors which are controlled by a motor controller through a computer. The computer acquires the measured S-parameters from the VNA for different stirrer positions.

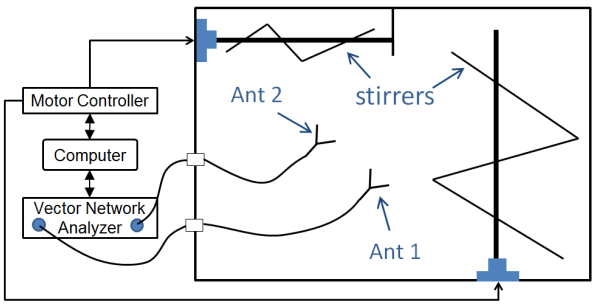

Fig. 1. Schematic plot of a typical RC measurement scenario.

Suppose the measured $S_{21}(\theta, f)$ is a complex function of the rotation angle θ of a stirrer and frequency f, the ACC (autocorrelation) is defined as [33-35]

This work was supported in part by the National Natural Science Foundation of China (61701224 and 61601219) and Nature Science Foundation of Jiangsu Province (BK20160804).

Q. Xu, L. Xing, Y. Zhao are with College of Electronic and Information Engineering, Nanjing University of Aeronautics and Astronautics, Nanjing 211106, China (e-mail: emxu@foxmail.com).

T.-H. Loh and M. Wang are with Engineering, Materials & Electrical Science Department, 5G & Future Communications Technology Group, National Physical Laboratory, Teddington, TW11 0LW, United Kingdom, (e-mail: tian.loh@npl.co.uk).

Y. Huang is with the Department of Electrical Engineering and Electronics, The University of Liverpool, Liverpool, L69 3GJ, UK. (e-mail: yi.huang@liv.ac.uk).

$$R(\partial\theta, f) = \int_{-\infty}^{\infty} S_{21}^{*}(\theta, f) S_{21}(\theta + \partial\theta, f) d\theta \qquad (1)$$

where * means the complex conjugate, $\partial\theta$ is the variable of the angular correlation. Without loss of generality, the upper and lower bound of the integral are written as ∞ and $-\infty$ respectively. Equation (1) is not limited to a rotated stirrer, it can also be applied to a sliding stirrer with variable distance ∂x (e.g. replacing $\partial\theta$ with ∂x). We can set $S_{21} = 0$ when θ is outside the defined angular range $[0, 360°]$ thus a rotated stirrer is treated the same as a sliding stirrer mathematically. In practice, the frequency stir can be applied to increase the sample number by smoothing the ACC over a certain frequency band. The average ACC can be obtained as $R_{avg}(\partial\theta, f) = \langle R(\partial\theta, f) \rangle_f$, where $\langle\cdot\rangle_f$ means averaging over a certain bandwidth.

III. Measurements

To measure the ACC of a stirrer, we rotated the vertical stirrer (V-stirrer) with a very fine rotation angle of 0.2 degrees/stirrer-step while keeping the horizontal stirrer (H-stirrer) standstill. The stirrers were driven by stepper motors with 6400 motor-steps/degree, which means 1280 motor-steps were triggered for a 0.2-degree stirrer rotation. *S*-parameters (S_{21}) of 1800 stirrer-steps were recorded for a 360-degree rotation. For each stirrer position, 16001 frequency points were measured in the frequency range of 10 MHz to 40 GHz (the full bandwidth of the VNA). Figure 2 shows the measurement scenario, Ant 1 and Ant 2 are wideband dipole antennas with return loss larger than 3 dB between 1 GHz and 40 GHz. Figure 3 shows the measured S_{21} for one stirrer position in the frequency range of 10 MHz ~ 40 GHz, and the measured S_{21} are at least 20 dB above the noise floor of the vector network analyzer (VNA) in 200 MHz ~ 40 GHz.

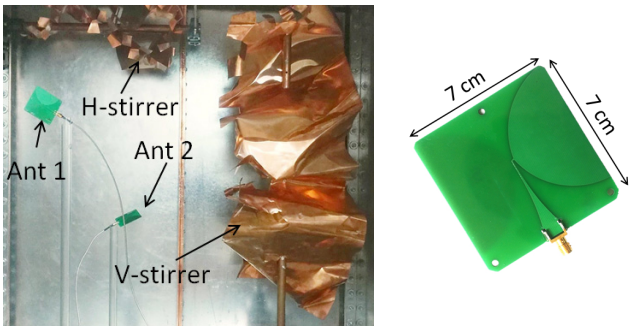

Fig. 2. Measurement scenario in an RC, the RC dimensions are 1.2 m (L) × 1.2 m (H) × 0.8 m (W), the lowest usable frequency is about 1 GHz. The diameter of the V-stirrer is 40 cm and the height is 1 m, the diameter of the H-stirrer is 20 cm and the length is 50 cm. The antennas are wideband dipole antennas shown in the right-hand side.

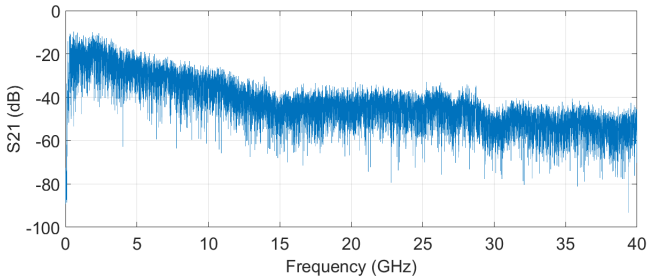

Fig. 3. The measured S_{21} at one stirrer position.

Using the measured S_{21}, the normalized average ACC $R_{navg}(\partial\theta, f)$ can be obtained by normalizing $R_{avg}(\partial\theta, f)$ to the peak values. The frequency stirring technique is applied to obtain $R_{navg}(\partial\theta, f)$, at each frequency of $R_{avg}(\partial\theta, f)$, the ACCs in a bandwidth of 200 MHz (i.e. $f \pm 100$ MHz) are used to obtain the average value, finally $R_{avg}(\partial\theta, f)$ is normalized to the peak value to obtain $R_{navg}(\partial\theta, f)$. The magnitude (Fig. 4(a)) and phase (Fig. 4(b)) of $R_{navg}(\partial\theta, f)$ are represented using the pseudo colors.

From Fig. 4(b), it is interesting to note that the phase of the ACC is nearly zero for correlated $\partial\theta$, thus the real part of R_{navg} dominates its value. This is because there is no phase biased for the ACC for different frequencies. When the frequency stir is applied, the random phases cancel each other and provide an unbiased value of zero degree.

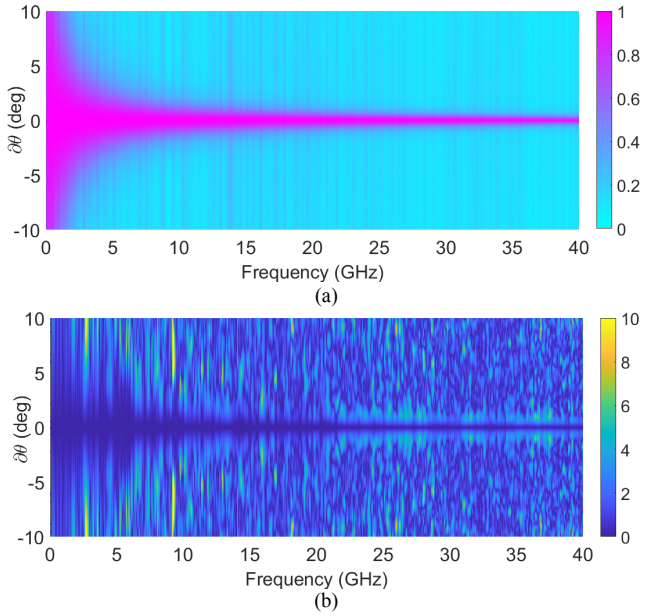

Fig.4. Measured $R_{navg}(\partial\theta, f)$ at different frequencies, (a) magnitude $|R_{navg}(\partial\theta, f)|$ and (b) phase ($|\angle R_{navg}(\partial\theta, f)|$) are represented using pseudo colors. Note that the V-stirrer was rotated while the H-stirrer was standstill.

Different from the ACC, the analytical form of the frequency correlation coefficient has already been obtained in [13]

$$|\langle R(\partial f) \rangle_m|_{norm} = \frac{1}{\sqrt{1 + (2\pi\tau_{RC}\partial f)^2}} \qquad (2)$$

where $\langle\cdot\rangle_m$ means averaging over different stirrer positions (mechanical stir), $norm$ means the frequency correlation is normalized to the peak value, τ_{RC} is the chamber decay constant, and ∂f is the variable of frequency correlation. Note that (2) can be derived analytically by using Wiener-Khinchin theorem from the time domain response of the RC [13, 36-37], as the power delay profile (PDP) in an RC has an analytical form of $P_0 e^{-t/\tau_{RC}}$ where P_0 is the PDP level when $t = 0$. Inspired from (2), we propose a closed-form expression for the ACC

$$R_{navg}(\partial\theta, f) = \frac{1}{\sqrt{1 + [\alpha(f)\partial\theta]^2}} \tag{3}$$

where $\alpha(f)$ in (1/deg) is a function of frequency which controls the correlation angle of R_{navg}.

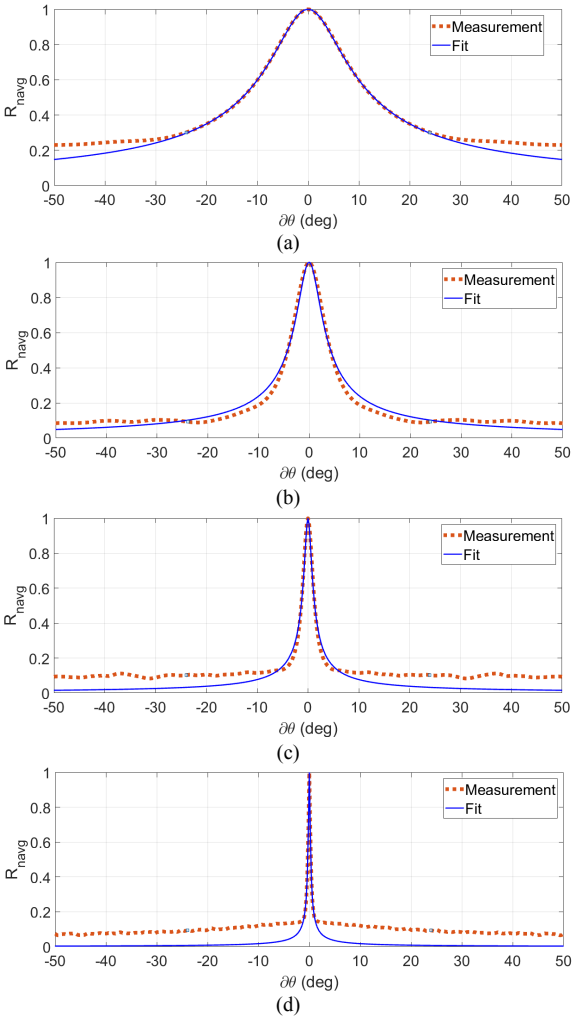

Fig. 5. Measured and fitted $R_{navg}(\partial\theta, f)$ at different frequencies, (a) f = 1 GHz, (b) f = 3 GHz, (c) f = 10 GHz, and (d) f = 40 GHz.

To obtain the model in (3), the least-squares fitting method is applied to calculate $\alpha(f)$ at each frequency to minimize the error between the analytical expression and the measured results. Because (3) is an approximated expression, it cannot fit the measured ACC perfectly in the whole range of $\partial\theta$ (from $-180°$ to $180°$). However, for small angles of $\partial\theta$, (3) is a very good approximation. We use a threshold value of $1/e \approx 0.37$ [26], and the least-squares fit is applied in the range of $R_{navg} > 0.37$. For large angles of $\partial\theta$, the correlation could be related to the shape of the stirrer and no simple analytical form could be obtained. Nevertheless, (3) can be regarded as a low order approximation for small $\partial\theta$. Figure 5(a)-(d) give the fitted results at 1 GHz, 3 GHz, 10 GHz and 40 GHz, respectively.

To estimate the accuracy, we compare the correlated angle obtained from the measured results and the analytical equation (analytical form in (3)), a threshold of $1/e$ is used. Figure 6 illustrates the fitted $\alpha(f)$ and the difference of the correlated angle $\Delta\theta$ obtained numerically and analytically. As can be seen, a very good agreement is obtained and the difference is less than 0.2 degrees at 40 GHz. The obtained analytical model is plotted in Fig. 7 which shows a very good agreement with Fig. 4(a).

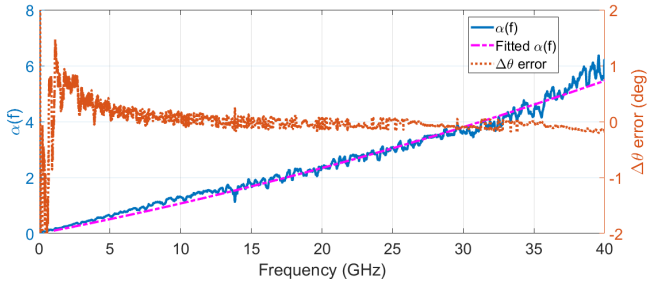

Fig. 6. $\alpha(f)$ and $\Delta\theta$ error in the measured frequency band, the V-stirrer was rotated. $\alpha(f) = 9.76 \times 10^{-2} f + 9.72 \times 10^{-4} f^2$, f in GHz.

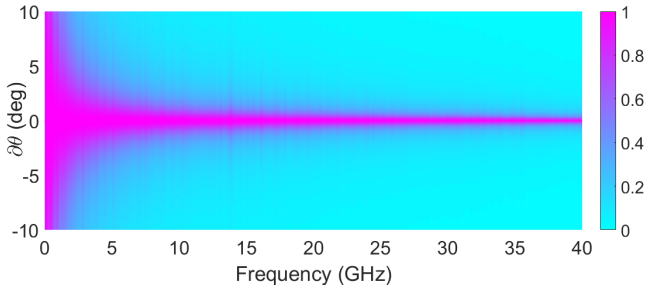

Fig. 7. Fitted $R_{navg}(\partial\theta, f)$ at different frequencies, the V-stirrer was rotated and the H-stirrer was still.

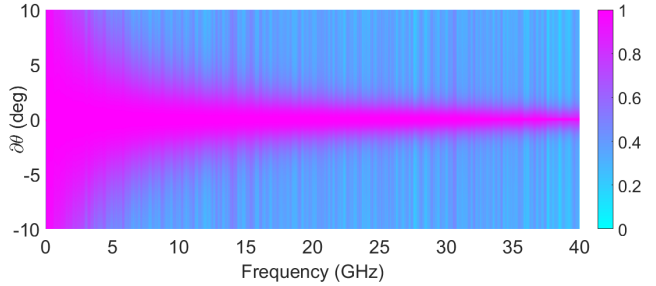

Fig. 8. Measured $R_{navg}(\partial\theta, f)$ at different frequencies, the H-stirrer was rotated and the V-stirrer was still.

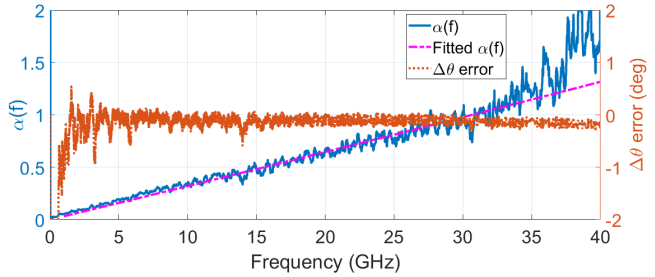

Fig. 9. $\alpha(f)$ and $\Delta\theta$ error in the measured frequency band, the H-stirrer was rotated with a still V-stirrer; a threshold value of $R_{navg} = 0.6$ was used to calculate the correlated angle. $\alpha(f) = 3.17 \times 10^{-2} f + 3.06 \times 10^{-5} f^2$, f in GHz.

We also repeated the measurement for a rotating H-stirrer with a standstill V-stirrer. The measured ACC is illustrated in Fig. 8, and the fitted $\alpha(f)$ is shown in Fig. 9 together with the error of $\Delta\theta$. Because the horizontal stirrer is smaller than the vertical one, a larger ACC is observed with color spread in $\partial\theta$-axis in Fig. 8, and a smaller $\alpha(f)$ is obtained compared with $\alpha(f)$ in Fig. 6. $\alpha(f)$ are also fitted using polynomials which show a nearly linear dependency with frequency at low frequencies.

IV. Properties of Average Angular Correlation

We have used a low order analytical expression to fit the ACC, and good agreements have been obtained for small angles. However, more properties can be obtained from (1).

A. Property I

When $\partial\theta = 0$,

$$R(0,f) = \int_{-\infty}^{\infty} S_{21}^*(\theta,f) S_{21}(\theta,f) d\theta = \int_0^{\Theta} |S_{21}(\theta,f)|^2 d\theta = \Theta \langle |S_{21}(f)|^2 \rangle_m \quad (4)$$

where $\langle\cdot\rangle_m$ means the average over different stirrer states and S_{21} is defined over the angular range of $[0, \Theta]$. As can be seen in (4), $\langle |S_{21}(f)|^2 \rangle_m$ is actually the chamber transfer function (including the insertion loss of antennas).

B. Property II

At each frequency, if we apply the Fourier transform to $S_{21}(\theta)$

$$s(\rho) = \mathcal{F}^{-1}[S_{21}^*(\theta)] = \int_{-\infty}^{\infty} S_{21}^*(\theta) e^{j2\pi\rho\theta} d\theta = \mathcal{F}[S_{21}(\theta)]^* = \left[\int_{-\infty}^{\infty} S_{21}(\theta) e^{-j2\pi\rho\theta} d\theta\right]^* \quad (5)$$

where $\mathcal{F}$ means the Fourier transform, ρ is the transformed variable of θ and s is the transformed S_{21}. By applying the Wiener-Khinchin theorem [13, 36-37] we have

$$|s(\rho)|^2 = |\mathcal{F}[S_{21}(\theta)]|^2 = \mathcal{F}^{-1}[R(\partial\theta)] \quad (6)$$

When $\rho = 0$, (6) becomes

$$|\mathcal{F}[S_{21}(\theta)]|^2_{\rho=0} = \left|\int_{-\infty}^{\infty} S_{21}(\theta) e^{-j2\pi\theta\rho} d\theta\right|^2_{\rho=0} = \mathcal{F}^{-1}[R(\partial\theta)]_{\rho=0} = \int_{-\infty}^{\infty} R(\partial\theta) e^{j2\pi\partial\theta\rho} d\partial\theta\Big|_{\rho=0} \quad (7)$$

Simplify (7), and note S_{21} is defined in the range of $\theta \in [0, \Theta]$, we have

$$\left|\int_0^{\Theta} S_{21}(\theta) d\theta\right|^2 = \Theta^2 |\langle S_{21}(\theta)\rangle_m|^2 = \int_{-\infty}^{\infty} R(\partial\theta) d\partial\theta \quad (8)$$

Note that the Rician K-factor is defined as [15-21]

$$K = \frac{|\langle S_{21}\rangle_m|^2}{\langle |S_{21,s}|^2\rangle_m} = \frac{|\langle S_{21}\rangle_m|^2}{\langle |S_{21} - \langle S_{21}\rangle_m|^2\rangle_m} \quad (9)$$

where $S_{21,s} = S_{21} - \langle S_{21}\rangle_m$ is the stirrer part of the S-parameters. When the unstirred part is small

$$K \approx \frac{|\langle S_{21}\rangle_m|^2}{\langle |S_{21}|^2\rangle_m} \quad (10)$$

Because $\langle |S_{21}|^2\rangle_m = R(0)$ varies slowly with frequency, from (4), (8) and (10), the mean value (over all angles) of the normalized ACC becomes

$$\bar{R}_{norm}(\partial\theta) = \frac{1}{2\Theta}\int_{-\Theta}^{\Theta} \frac{R(\partial\theta)}{R(0)} d\partial\theta = \frac{\Theta^2 |\langle S_{21}(\theta)\rangle_m|^2}{2\Theta^2 \langle |S_{21}(\theta)|^2\rangle_m} \approx \frac{K}{2} \quad (11)$$

where $\bar{R}_{norm}(\partial\theta)$ represents the mean value of the normalized ACC.

Interestingly, the mean value of the normalized R is half of the K-factor. This proves the equivalency of the K-factor and the normalized ACC, also if the average normalized ACC is used we have

$$\bar{R}_{navg}(\partial\theta) \approx \frac{\langle K\rangle_f}{2} \quad (12)$$

for K-factors, where $\bar{R}_{navg}(\partial\theta)$ represents the mean value of the normalized ACC averaged over frequency, and $\langle K\rangle_f$ means K-factor averaging over frequency. Also note when the K-factor is small, we have $\langle K\rangle_f = \mathrm{ACS}_{all}/(\mathrm{ACS}_{all} + \mathrm{TSCS})$, where ACS_{all} is the equivalent ACS for all the loss in the RC and the TSCS is measured total scattering cross section of the stirrer in the RC [37]. $\bar{R}_{navg}(\partial\theta)$ can be linked to the intrinsic properties of the RC in a similar way (with a factor of 1/2).

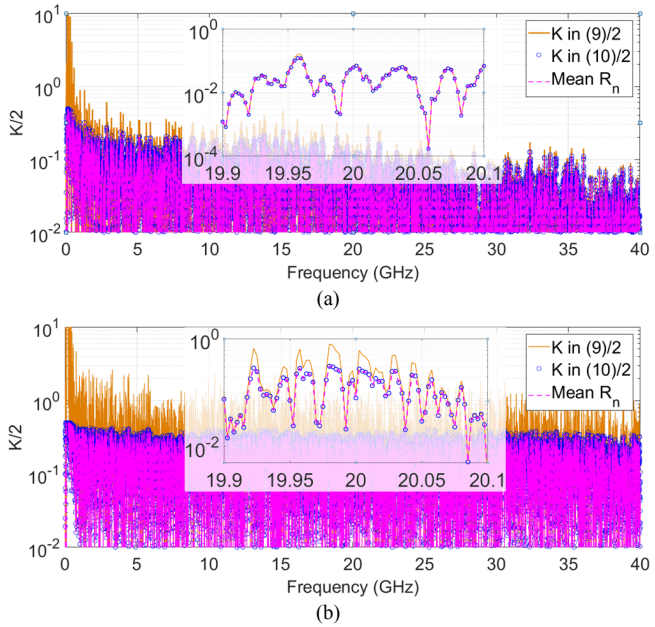

Fig. 10. Equation (9), (10), and (11) are used to calculate the *K*-factor, 19.9 GHz ~ 20.1 GHz is zoomed in; (a) the V-stirrer is rotated with a still H-stirrer; (b) the H-stirrer is rotated with a still V-stirrer.

Equation (11) is verified in Fig. 10, the *K*-factors are calculated using both (9) and (10) for the V- and H-stirrers. As can be seen, because the V-stirrer is larger than the H-stirrer, this leads to small *K*-factors, and the difference between (9) and (10) is ignorable. For the small H-stirrer, the unstirred part is significant, thus a clear difference is observed between (9) and (10) for large *K*-factors. However, because (11) is derived using (10), good agreements between (11) and (10) are obtained for both V-and H-stirrers.

C. *Property III*

In some references [1, 29, 38], at each frequency, the autocorrelation is defined as

$$R_0(\partial\theta) = \int_{-\infty}^{\infty}[S_{21}^*(\theta) - \langle S_{21}^*(\theta)\rangle][S_{21}(\theta+\partial\theta) - \langle S_{21}(\theta+\partial\theta)\rangle]d\theta \quad (13)$$

where the mean value of $S_{21}(\theta)$ is deducted and we use R_0 to represent the autocorrelation of S_{21} with zero means. It would be necessary to compare these two definitions in (1) and (13). We can find that definitions in (1) and (13) can be related using *K*-factor. If we expand (13), we have

$$R_0(\partial\theta) = \int_{-\infty}^{\infty} S_{21}^*(\theta)S_{21}(\theta+\partial\theta)d\theta - |\langle S_{21}(\theta)\rangle_m|^2\Theta = R(\partial\theta) - |\langle S_{21}(\theta)\rangle_m|^2\Theta \quad (14)$$

After normalization, (14) becomes

$$R_{0norm}(\partial\theta) = \frac{R_0(\partial\theta)}{R_0(0)} = \frac{R(\partial\theta) - |\langle S_{21}(\theta)\rangle_m|^2\Theta}{R(0) - |\langle S_{21}(\theta)\rangle_m|^2\Theta} \quad (15)$$

Substituting (4) into (15) and applying (10) for small *K*-factors, we have

$$R_{0norm}(\partial\theta) = \frac{\frac{R(\partial\theta)}{R(0)} - \frac{|\langle S_{21}(\theta)\rangle_m|^2}{\langle|S_{21}(f)|^2\rangle_m}}{1 - \frac{|\langle S_{21}(\theta)\rangle_m|^2}{\langle|S_{21}(f)|^2\rangle_m}} \approx \frac{R_{norm}(\partial\theta) - K}{1-K} \quad (16)$$

where $R_{norm}(\partial\theta)$ is the normalized $R(\partial\theta)$. From (16), the relationship between definitions in (1) and (13) is clear. The measured normalized ACC at 40 GHz is used to verify (16); the left-hand side and the right-hand side of (16) for the H-stirrer and the V-stirrer are illustrated in Fig. 11. As expected, they agree well.

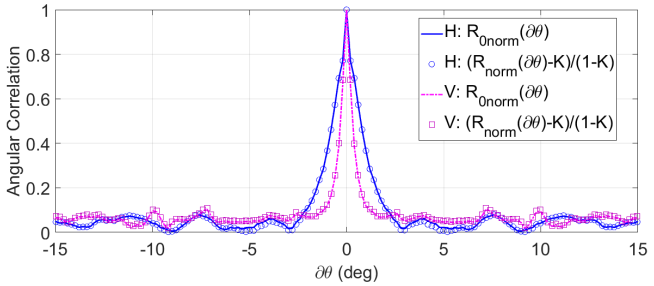

Fig. 11. Measured normalized ACC in (16) at 40 GHz for H- and V-stirrer, the left-hand side and the right-hand side of (16) are compared, the *K*-factors are -14.8 dB and -10.6 dB for the H- and V-stirrer respectively.

V. Discussion and Conclusions

To investigate the angular correlation of a mechanical stirrer, a very fine stirrer rotation angle has been used (0.2 degrees/stirrer-step). The measurement time was relatively long, which took about 10 hours for a whole rotation (1800 stirrer-steps).

An analytical expression has been proposed to fit ACC which shows good agreements with measurement results for small angles. The proposed analytical expression compresses the measurement data: conventionally, the ACC needs to be characterized as a function of both $\partial\theta$ and f, but now one analytical expression is enough. The fitted $\alpha(f)$ characterizes the ACC for different frequencies with very small errors. Some general properties of the ACC have been detailed; an interesting finding is that the mean value of the normalized ACC equals a half of the *K*-factor, which proves the equivalency of the mean angular correlation and the *K*-factor. Different definitions for the autocorrelation have also been compared and related by using the *K*-factor.

We also note that the approximate form for (3) could not be unique, an alternative approximate form proposed in [39] for the correlation (for the temperature fluctuation in the ocean) in distance x is

$$R(x) = e^{-x^2/a^2} \quad (17)$$

If we check the Taylor series for (3) and (17), and let $a = \sqrt{2}/\alpha$, we have

$$\frac{1}{\sqrt{1+(\alpha x)^2}} = 1 - \frac{1}{2}(\alpha x)^2 + \frac{3}{8}(\alpha x)^4 + O(x^6) \quad (18)$$

$$e^{-x^2/a^2} = 1 - \frac{1}{2}(\alpha x)^2 + \frac{1}{8}(\alpha x)^4 + O(x^6) \quad (19)$$

The difference between (18) and (19) is on the order of $(\alpha x)^4/4$, which is very small in the correlated region (by replacing x with $\partial\theta$). Another form proposed in [39] is $e^{-|x|/a}$, but the derivative of this expression for $x = 0$ is not zero, thus it is not suitable for this application.

If we check (12) carefully, an interesting phenomenon can be observed. Because the integral of R_{navg} over all the angles is a finite value ($\Theta\langle K\rangle_f$ in (12)), while the correlated angle drops down very quickly for small $\partial\theta$, thus the contribution of the integral $\int_{-\Theta}^{\Theta} R_{navg}\, d\partial\theta$ is mainly from a large $\partial\theta$. Fig. 12 shows the measured R_{navg} at 40 GHz for two stirrers. It is interesting to note that although the ACC drops quickly from the peak value, $\Theta\langle K\rangle_f$ is a finite number, thus it is impossible to have a curve of R_{navg} with both a sharp roll-off and nearly zero correlations for a large $\partial\theta$. This phenomenon was not noticed before, and the correlation drops down slowly for large $\partial\theta$. This effect is very significant at high frequencies because the contribution to $\int_{-\Theta}^{\Theta} R_{navg}\, d\partial\theta$ from the tip of the curve (in Fig. 12) is very small.

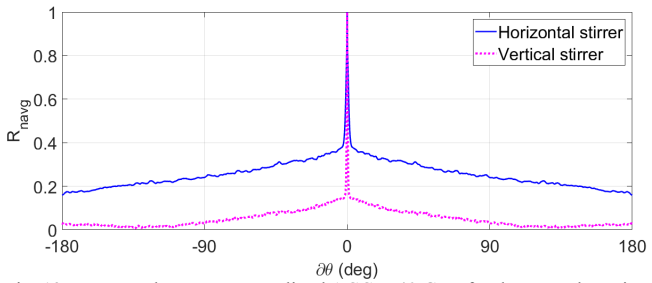

Fig. 12. Measured average normalized ACC at 40 GHz for the rotated H-stirrer and V-stirrer. $\partial\theta$ in the range of $[-180°, 180°]$ is shown to have a understanding of R_{navg} for a large $\partial\theta$.

From this study, a parameter (average Rician *K*-factor) in communication channel emulation is well linked to a physical quantity (ACC) in an RC. By applying this relationship, we can emulate communication channels in an RC using a small stirrer to create controlled correlated channels or measure the average *K*-factors using the average ACC of a rotating stirrer.

REFERENCES

[1] D. A. Hill, Electromagnetic Fields in Cavities: Deterministic and Statistical Theories, Wiley-IEEE Press, 2009.

[2] P. -S. Kildal, "Preparing for GBit/s coverage in 5G: Massive MIMO, PMC packaging by gap waveguides, OTA testing in random-LOS," *Loughborough Antennas & Propagation Conference (LAPC)*, Loughborough, UK, 2015, pp. 1-5.

[3] C. S. P. Lötbäck, "Extending the frequency range of reverberation chamber to millimeter waves for 5G over-the-air testing," *11th European Conference on Antennas and Propagation (EUCAP)*, Paris, France, 2017, pp. 3012-3016.

[4] P. -S. Kildal and A. A. Glazunov, "OTA testing of 3G-5G devices with MIMO: From anechoic chambers to reverberation chambers and … back again?" *IEEE International Symposium on Antennas and Propagation & USNC/URSI National Radio Science Meeting*, San Diego, USA, 2017, pp. 1697-1698.

[5] C. P. Lötbäck, K. Arvidsson, M. Högberg and M. Gustafsson, "Base station over-the-air testing in reverberation chamber," *11th European Conference on Antennas and Propagation (EUCAP)*, Paris, France, 2017, pp. 628-632.

[6] K. A. Remley, H. Fielitz, H. A. Shah and C. L. Holloway, "Simulating MIMO techniques in a reverberation chamber," *IEEE International Symposium on Electromagnetic Compatibility*, Long Beach, CA, USA, 2011, pp. 676-681.

[7] C. L. Holloway, H. A. Shah, R. J. Pirkl, W. F. Young, D. A. Hill and J. Ladbury, "Reverberation chamber techniques for determining the radiation and total efficiency of antennas," *IEEE Transactions on Antennas and Propagation*, vol. 60, no. 4, pp. 1758–1770, Apr. 2012.

[8] L. R. Arnaut and G. Gradoni, "Probability distribution of the quality factor of a mode-stirred reverberation chamber," *IEEE Transactions on Electromagnetic Compatibility*, vol. 55, no. 1, pp. 35-44, Feb. 2013.

[9] L. R. Arnaut, M. I. Andries, J. Sol and P. Besnier, "Evaluation method for the probability distribution of the quality factor of mode-stirred reverberation chambers," *IEEE Transactions on Antennas and Propagation*, vol. 62, no. 8, pp. 4199-4208, Aug. 2014.

[10] A. Gifuni, G. Ferrara, M. Migliaccio and A. Sorrentino, "Estimate of the probability density function of the quality factor of mode tuned, source stirred and mode stirred reverberation chambers," *IEEE Transactions on Electromagnetic Compatibility*, vol. 57, no. 5, pp. 926-936, Oct. 2015.

[11] A. Gifuni, "Probability density function of the quality factor for reverberation chambers operating with hybrid stirring including frequency stirring," *IEEE Transactions on Electromagnetic Compatibility*, vol. 58, no. 3, pp. 919-922, Jun. 2016.

[12] L. R. Arnaut, P. Besnier, J. Sol and M. I. Andries, "On the uncertainty quantification of the quality factor of reverberation chambers," *IEEE Transactions on Electromagnetic Compatibility*, 2018, doi: 10.1109/TEMC. 2018.2839345.

[13] C. L. Holloway, H. A. Shah, R. J. Pirkl, K. A. Remley, D. A. Hill and J. Ladbury, "Early time behavior in reverberation chambers and its effect on the relationships between coherence bandwidth, chamber decay time, RMS delay spread, and the chamber buildup time," *IEEE Transactions on Electromagnetic Compatibility*, vol. 54, no. 4, pp. 714-725, Aug. 2012.

[14] Q. Xu, Y. Huang, L. Xing and Z. Tian, "Extract the decay constant of a reverberation chamber without satisfying Nyquist criterion," *IEEE Microwave and Wireless Components Letters*, vol. 26, no. 3, pp. 153-155, March 2016.

[15] C. L. Holloway, D. A. Hill, J. M. Ladbury, P. F. Wilson, G. Koepke and J. Coder, "On the use of reverberation chambers to simulate a Rician radio environment for the testing of wireless devices," *IEEE Transactions on Antennas and Propagation*, vol. 54, no. 11, pp. 3167-3177, Nov. 2006.

[16] C. M. J. Wang, K. A. Remley, A. T. Kirk, R. J. Prikl, C. L. Holloway, D. F. Williams and P. D. Hale, "Parameter estimation and uncertainty evaluation in a low Rician K-factor reverberation-chamber environment," *IEEE Transactions on Electromagnetic Compatibility*, vol. 56, no. 5, pp. 1002-1012, Oct. 2014.

[17] M. I. Andries, P. Besnier and C. Lemoine, "Estimating K-factor and time spread parameters from a transient response of a pulse modulated sine wave in reverberation chamber," *IEEE Transactions on Antennas and Propagation*, vol. 61, no. 1, pp. 380-389, Jan 2013.

[18] C. Lemoine, E. Amador and P. Besnier, "Mode-stirring efficiency of reverberation chambers based on Rician K-factor," *Electronics Letters*, vol. 47, no. 20, pp. 1114-1115, Sep. 2011.

[19] C. Lemoine, E. Amador and P. Besnier, "On the K-factor estimation for Rician channel simulated in reverberation chamber," *IEEE Transactions on Antennas and Propagation*, vol. 59, no. 3, pp. 1003-1012, Mar. 2011.

[20] A. Sorrentino, S. Cappa, A. Gifuni, G. Ferrara and M. Migliaccio, "The rice K-factor distribution within a mode-stirred reverberating chamber," *International Symposium on Electromagnetic Compatibility - EMC EUROPE*, Angers, France, 2017, pp. 1-5.

[21] X. Chen, P. -S. Kildal and S. H. Lai, "Estimation of average Rician K-factor and average mode bandwidth in loaded reverberation chamber," *IEEE Antennas and Wireless Propagation Letters*, vol. 10, pp. 1437-1440, 2011.

[22] U. Calberg, P. –S. Kildal, A. Wofgang, O. Sotoudeh and C. Orlenius, "Calculated and measured absorption cross sections of lossy objects in reverberation chamber," *IEEE Transactions on Electromagnetic Compatibility*, vol. 46, no. 2, pp. 146-154, May 2004.

[23] I. D. Flintoft, G. C. R. Melia, M. P. Robinson, J. F. Dawson and A. C. Marvin, “Rapid and accurate broadband absorption cross-section measurement of human bodies in a reverberation chamber,” *Measurement Science and Technology*, vol. 26, no. 6, pp. 65701-65709, Jun. 2015.

[24] I. D. Flintoft, S. J. Bale, S. L. Parker, A. C. Marvin, J. F. Dawson and M. P. Robinson, “On the measurable range of absorption cross section in a reverberation chamber,” *IEEE Transactions on Electromagnetic Compatibility*, vol. 58, no. 1, pp. 22-29, Feb. 2016.

[25] Q. Xu, Y. Huang, L. Xing, Z. Tian, J. Zhou, A. Chen and Y. Zhuang., “Average absorption coefficient measurement of arbitrarily shaped electrically large objects in a reverberation chamber,” *IEEE Transactions on Electromagnetic Compatibility*, vol. 58, no. 6, pp. 1776-1779, Dec. 2016.

[26] IEC 61000-4-21, Electromagnetic compatibility (EMC) – Part 4-21: Testing and measurement techniques – Reverberation chamber test methods, IEC Standard, Ed 2.0, 2011-01.

[27] A. Sorrentino, G. Ferrara and M. Migliaccio, “On the coherence time control of a continuous mode stirred reverberating chamber,” *IEEE Transactions on Antennas and Propagation*, vol. 57, no. 10, pp. 3372-3374, Oct. 2009.

[28] F. Moglie and V. M. Primiani, “Analysis of the independent positions of reverberation chamber stirrers as a function of their operating conditions,” *IEEE Transactions on Electromagnetic Compatibility*, vol. 53, no. 2, pp. 288-295, May 2011.

[29] R. J. Pirkl, K. A. Remley and C. S. L. Patane, “Reverberation chamber measurement correlation,” *IEEE Transactions on Electromagnetic Compatibility*, vol. 54, no. 3, pp. 533-545, Jun. 2012.

[30] X. Chen, “On independent platform sample number for reverberation chamber measurements,” *IEEE Transactions on Electromagnetic Compatibility*, vol. 54, no. 6, pp. 1306-1309, Dec. 2012.

[31] G. Gradoni, V. M. Primiani and F. Moglie, “Carousel stirrer efficiency evaluation by a volumetric lattice-based correlation matrix,” *IEEE International Symposium on Electromagnetic Compatibility*, Denver, CO, 2013, pp. 819-824.

[32] G. Gradoni, F. Moglie and V. M. Primiani, “Correlation matrix methods to assess the stirring performance of electromagnetic reverberation chambers,” *Wave Motion*, accepted, 2018. https://doi.org/10.1016/j.wavemoti.2018.09.008.

[33] K. Karlsson, X. Chen, P. S. Kildal and J. Carlsson, “Doppler spread in reverberation chamber predicted from measurements during step-wise stationary stirring,” *IEEE Antennas and Wireless Propagation Letters*, vol. 9, pp. 497-500, 2010.

[34] X. Chen, P. S. Kildal and J. Carlsson, “Determination of maximum Doppler shift in reverberation chamber using level crossing rate,” *Proceedings of the 5th European Conference on Antennas and Propagation (EUCAP)*, Rome, Italy, 2011, pp. 62-65.

[35] J. H. Choi, J. H. Lee and S. O. Park, “Characterizing the impact of moving mode-stirrers on the Doppler spread spectrum in a reverberation chamber,” *IEEE Antennas and Wireless Propagation Letters*, vol. 9, pp. 375-378, 2010.

[36] E. W. Weisstein, “Wiener-Khinchin Theorem.” From MathWorld--A Wolfram Web Resource. http://mathworld.wolfram.com/Wiener-KhinchinTheorem.html.

[37] Q. Xu, L. Xing, Y. Zhao, Z. Tian and Y. Huang, “Wiener–Khinchin theorem in a reverberation chamber,” *IEEE Transactions on Electromagnetic Compatibility*, accepted, 2018. doi: 10.1109/TEMC.2018.2863297.

[38] A. Ishimaru, Wave Propagation and Scattering in Random Media, Wiley-IEEE Press, 1997.

[39] L. A. Chernov, Wave Propagation in a Random Medium, Dover Publications, New York, 2017.